 Bull. Chem. Soc. Jpn., **76**, 271–281 (2003)

Flux Correlation Approach to Thermal Reactions and Recombination Rates

Koichi Saito

Tohoku Pharmaceutical University, 4-4-1 Komatsushima, Aoba-ku, Sendai 981-8558

(Received May 22, 2002)

The rate constants for recombination and exchange processes are studied in terms of two different flux correlation approaches: one is the Yamamoto approach, which is based on the linear response theory, and the other is the Miller one. Using those approaches we consider two exactly solvable cases, i.e., the free particle and the parabolic potential models. Since the rate constants for recombination and exchange processes are calculated by Laplace transforms of the flux correlation functions, the two approaches give different results. In the present calculation, we find that the rate constant in the Yamamoto approach is larger than that in the Miller approach by about 40% at low temperature (∼100 K) and high pressure (∼1 GPa). The difference is considerable in the region where quantum effects dominate.

When one wants to study a chemical reaction at the most detailed level, it is necessary to calculate the Schrödinger equation for a state-to-state differential scattering cross section, which is a function of total energy E and total angular momentum J. Such quantum reactive scattering cross sections have actually been studied for simple chemical reactions, where a time-dependent scattering formalism based on the S-matrix Kohn variational approach[1] or a coupled channel method in hyperspherical coordinates[2] has usually been used.

However, in chemical applications, there are many cases where only the (microcanonical or canonical) rate constant for a reaction is needed. If the full, state-to-state scattering calculation has been carried out, the rate constant is, of course, given by an average of the cross sections. If it is, however, *only* the rate constant that is desired, such a complete calculation for all state-to-state information is *not* economical. Furthermore, because of the rapid growth of the number of open vibration-rotation channels with increasing thermally accessible collision energies, the calculation of a rate constant via exact quantum state-to-state calculations would not be feasible even for a simple reaction.

The traditional way of evaluating a rate constant is the transition state theory (TST).[3] However, TST is a *classical* theory and it is approximate, because it does not involve the effect of *recrossing* of the system over the transition state dividing a potential surface. A number of improvements have been proposed to take the recrossing effect into account.[4,5]

In the early 60's, Yamamoto[6] first formulated an exact expression for the rate constant as an application of the general statistical mechanical theory of irreversible process, which was established by Kubo et al.[7] and Mori.[8] Later (in the early 70's), Miller et al.[5,9] separately developed a method for the rate constant using a time integral of the flux–flux autocorrelation function, which is exact in the limit that the dynamics is extended to $t \to \infty$. Because the flux-flux correlation is calculated via time-dependent quantum mechanics, the feasibility of this approach depends on how to evaluate the Hamiltonian, flux and time evolution operators for the system. The flux–flux autocorrelation function method has been applied to a variety of chemical reactions.[10] In particular, the reaction of $H + H_2$ has been studied intensively.[11]

It has recently been shown how a quantum mechanical version of the Lindemann mechanism for collisional recombination

$$\mathrm{A + B} \rightleftharpoons \mathrm{AB^*}, \tag{1}$$

$$\mathrm{AB^* + M} \rightarrow \mathrm{AB + M}, \tag{2}$$

can be handled by the flux–flux autocorrelation function for the A–B collision.[10,12,13] Here the process is affected by the bath gas M. Some applications of this new theory are listed in Ref. 14. It is furthermore possible to generalize the formalism to include chemical reactions as well as recombination:

$$\mathrm{A + BC} \rightleftharpoons \mathrm{ABC^*} \rightarrow \mathrm{AB + C}, \tag{3}$$

$$\mathrm{ABC^* + M} \rightarrow \mathrm{ABC + M}. \tag{4}$$

Equations 3 and 4 simultaneously describe the recombination process (A + BC → ABC) and the exchange reaction (A + BC → AB + C).[13] This method has been applied to the interesting (combustion) reactions ($O + OH \rightleftharpoons H + O_2$) and the recombination reactions ($O + OH + M \rightarrow HO_2 + M \leftarrow H + O_2 + M$). Those reactions are very important in atmospheric chemistry.[15]

The purpose of this paper is to study the difference between the way proposed by Yamamoto,[6] which is based on the linear response theory or the so-called Kubo formula,[7] and the flux–flux autocorrelation function method proposed by Miller et al.[5,9] The two approaches can provide the same result to the rate constant for a simple chemical reaction, because it is given in terms of the integral of the flux-flux correlation function with respect to time.[5,9] However, the shapes of the correlation

functions calculated by the two methods are quite different from each other. For the recombination and exchange reactions (like Eqs. 3 and 4), the rate constants in the two approaches could be different because they are evaluated by Laplace transforms of the flux-flux correlation functions. It is expected that the difference will appear in the region where quantum effects dominate.

In this paper, we first review the correlation function method briefly and show the difference between Yamamoto's and Miller's approaches explicitly. The rate constants for recombination and exchange processes are also discussed. Next, we study two exactly solvable cases, i.e., the free particle and the parabolic potential models. Finally, the summary and conclusion are given.

1 Flux–Flux Correlation Approach to Rate Constants

In the *classical* limit, a rate constant is generally given by an average of the *flux* through some dividing surface that separates reactants from products (see Fig. 1). The canonical rate constant is then given by[10,#]

$$k_{cl}(T) = Q_r(T)^{-1}(2\pi)^{-f}\int \mathrm{d}\vec{p}_1\int \mathrm{d}\vec{q}_1\, e^{-\beta H(\vec{p}_1,\vec{q}_1)}F(\vec{p}_1,\vec{q}_1)\mathscr{P}(\vec{p}_1,\vec{q}_1), \tag{5}$$

where $\beta^{-1} = k_B T$ (T, temperature) and $(\vec{p}_1,\vec{q}_1)$ provides the initial conditions of the momenta and (reaction) coordinates for classical trajectories of the system (consisting of f degrees of freedom). The system is described by the Hamiltonian $H(\vec{p}_1,\vec{q}_1)$. Here $Q_r(T)$ is the partition function per unit volume for the noninteracting reactants and F is the flux factor which describes the trajectories crossing the dividing surface specified by $s(\vec{q}) = 0$:

$$F(\vec{p}_1,\vec{q}_1) = \frac{\mathrm{d}}{\mathrm{d}t}h(s(\vec{q})) = \delta(s(\vec{q}))v_s, \tag{6}$$

where $s(\vec{q})$ is some function of position $\vec{q}$ that is negative on the reactant side and positive on the product side. Then, $h(s)$ is the step function, which is $+1(0)$ for $s > (<)0$, and v_s is the normal component of the velocity to the dividing surface $s(\vec{q})$. The factor $\mathscr{P}$ in Eq. 5 involves all information of the dynamics and it is unity when the trajectory is on the product side in the infinite future and zero otherwise. This implies that it is given by

$$\mathscr{P}(\vec{p}_1,\vec{q}_1) = \lim_{t\to\infty}h(s(\vec{q}(t))) = \int_0^\infty \mathrm{d}t\frac{\mathrm{d}}{\mathrm{d}t}h(s(\vec{q}(t))) = \int_0^\infty \mathrm{d}t F(\vec{p}(t),\vec{q}(t)), \tag{7}$$

where Eq. 6 is used. Thus, $\mathscr{P}$ provides the probability that the trajectory lies on the product side of the dividing surface at $t \to \infty$. The rate constant then reads

$$Q_r k_{cl}(T) = \int_0^\infty \mathrm{d}t\, C_{cl}(t), \tag{8}$$

where

$$C_{cl}(t) = (2\pi)^{-f}\int \mathrm{d}\vec{p}_1\int \mathrm{d}\vec{q}_1\, e^{-\beta H(\vec{p}_1,\vec{q}_1)}F(\vec{p}_1,\vec{q}_1)F(\vec{p}(t),\vec{q}(t)). \tag{9}$$

This means that the rate constant is calculated by the time integral of the flux–flux autocorrelation function $C_{cl}(t)$.

We use the natural unit, i.e., $h/2\pi = c = 1$.

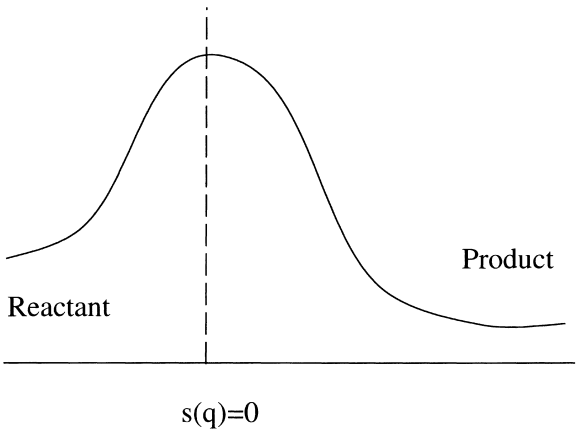

Fig. 1. Sketch of a potential surface in one-dimensional reaction versus the reaction coordinate q.

To take quantum effects into account, it is necessary to replace the phase space integral by a quantum trace representation. In the linear response theory,[7] the response functon is usually defined as

$$\phi_{BA}(t) = -i\mathrm{tr}(\rho[A, B(t)]), \tag{10}$$

where $\rho = e^{-\beta H}/\mathrm{tr}(e^{-\beta H})$ is the density operator for an equilibrium state. After the perturbation by the operator A at $t = 0$, the response of the quantity $B(t)$ ($= e^{itH}Be^{-itH}$) at time t in the system is described by the response function $\phi_{BA}(t)$. For the flux–flux autocorrelation function, one can identify that $A = h(s)$ and $B(t) = F(t)$. Here $F(0)$ is the flux operator at $t = 0$, which is given by[9]

$$F(0) = i[H,h(s)] = \frac{1}{2}\left[\frac{p}{m}\delta(s) + \delta(s)\frac{p}{m}\right], \tag{11}$$

with p the momentum operator and m the reduced mass of the system. Thus, the response function for the rate constant is

$$\phi_{Fh}(t) = -i\mathrm{tr}(\rho[h(s), F(t)]). \tag{12}$$

Using the Kubo identity[7]

$$[A,e^{-\beta H}] = e^{-\beta H}\int_0^\beta \mathrm{d}\lambda\, e^{\lambda H}[H,A]e^{-\lambda H}, \tag{13}$$

the response function reads

$$\phi_{Fh}(t) = \int_0^\beta \mathrm{d}\lambda\, \mathrm{tr}(\rho F(-i\lambda)F(t)), \tag{14}$$

where Eq. 11 is used and $F(-i\lambda) = e^{\lambda H}F(0)e^{-\lambda H}$.

In the linear response theory, the relaxation function Φ_{BA} is defined as

$$\Phi_{BA}(t) = \lim_{\varepsilon\to 0}\int_t^\infty \mathrm{d}s\, \phi_{BA}(s)e^{-\varepsilon s}. \tag{15}$$

The relaxation function for the rate constant is thus given by

$$\Phi_{Fh}(t) = \int_t^\infty \mathrm{d}s\, \phi_{Fh}(s) = \int_t^\infty \mathrm{d}s\int_0^\beta \mathrm{d}\lambda\, \mathrm{tr}(\rho F(-i\lambda)F(s)), \tag{16}$$

where we assumed that the response function decreases rapidly as $t \to \infty$. The rate constant in quantum mechanics is now given in terms of the relaxation function at $t = 0$

$$Q_r k(T) = \beta^{-1}\Phi_{Fh}(0) = \beta^{-1}\int_0^\infty dt \int_0^\beta d\lambda \, \mathrm{tr}(\rho F(-i\lambda)F(t)) \equiv \int_0^\infty dt \, C(t), \tag{17}$$

where the flux–flux autocorrelation function in quantum mechanics $C(t)$ is defined by

$$C(t) = \beta^{-1}\int_0^\beta d\lambda \, \mathrm{tr}(e^{-\beta H}F(-i\lambda)F(t)). \tag{18}$$

In the present notation, $C(t)$ in Eq. 18 corresponds to the flux correlation proposed by Yamamoto.[6] We should note that there exists an integral with respect to λ which stems from the Kubo identity and that it is dispensable in the *classical* limit $\beta \to 0$. Because it is more convenient to use the commutation relation in Eq. 12 rather than Eq. 18 in actual calculations, we re-define the Yamamoto's correlation function by

$$C^Y(t) = \frac{1}{i\beta}\mathrm{tr}(e^{-\beta H}[h(s), F(t)]), \tag{19}$$

where the superscript Y stands for "Yamamoto".

By contrast, in Miller's approach[5,9] the variable λ in the flux is fixed to be $\beta/2$ and the λ integral is performed. Thus, from Eq. 18 Miller's correlation function is given by

$$C^M(t) = \mathrm{tr}(F(0)e^{it_c^* H}F(0)e^{-it_c H}), \tag{20}$$

where $t_c = t - i\beta/2$ and the superscript M stands for "Miller". This modification certainly makes actual calculations simple, because the flux operators are involved symmetrically in the correlation function. In fact, Yamamoto's correlation function $C^Y(t)$ is *not* identical to $C^M(t)$. However, their integrals with respect to time are identical to each other, and hence they can provide the same rate constant. Therefore, the way of Miller et al.[5,9] certainly has some distinct advantages in actual numerical calculations.

2 Rate Constants for Recombination and Exchange Reactions

It is possible to generalize the flux correlation approach to treat recombination and exchange reactions.[10,12,13] It may be intuitive and useful to begin with the classical description of the process again. Let us consider the reaction of A + BC → AB + C and ABC (see Fig. 2). The classical rate constants for the exchange (A + BC → AB + C) and recombination (A + BC → ABC) reactions are again given by Eq. 5, i.e., averages of the flux $F_r(\vec{p}_1, \vec{q}_1)$ and the probability $\mathscr{P}(\vec{p}_1, \vec{q}_1)$ over the Boltzmann distribution. Here F_r is the flux at the reactant dividing surface s_r (see Fig. 2):

$$F_r = \frac{d}{dt}h(s_r) = \delta(s_r)v_r. \tag{21}$$

Note that $h(s_r)$ is again the step function, which is 0(1) for position $\vec{q}$ to the left (right) of the dividing surface s_r, and that v_r is the normal component of the velocity to the surface s_r. Similarly we define the step function for the product dividing surface s_p by $h(s_p)$ (see Fig. 2), that is, $h(s_p) = 0(1)$ for position $\vec{q}$ to the left (right) of the dividing surface s_p. The difference of those step functions, $h_c(\vec{q}) = h(s_r(\vec{q})) - h(s_p(\vec{q}))$, is unity for position $\vec{q}$ between the two dividing surfaces (i.e., in the "compound" region) and zero outside.

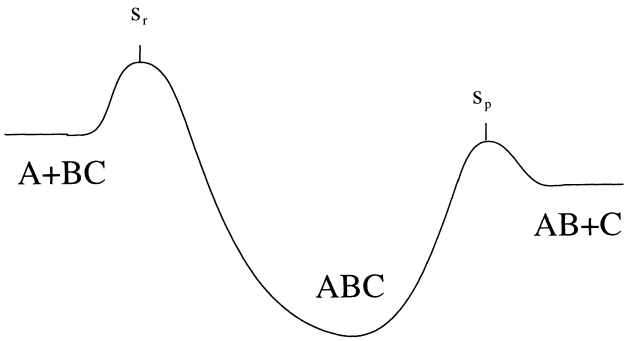

Fig. 2. One-dimensional schematic diagram of the interaction potential for the A + BC → AB + C reaction. The compound region, ABC, is bounded by the dividing surfaces on reactant (s_r) and product (s_p) sides.

Because the probability of the system experiencing a deactivating ($ABC^* + M \to ABC + M$) collision with the bath gas M can be evaluated by $1 - e^{-\eta t}$ at time t (η describes the frequency of deactivating collisions and it depends on pressure P and T of the bath gas), the recombination probability is estimated as

$$\mathscr{P}_{\mathrm{rec}} = 1 - e^{-\eta\tau}, \tag{22}$$

where τ is the time the trajectory (it is on s_r at $t = 0$) is in the compound region. Thus, using h_c and an integration by parts, $\mathscr{P}_{\mathrm{rec}}$ reads[13]

$$\begin{aligned}\mathscr{P}_{rec} &= \int_0^\infty dt \, h_c(\vec{q}(t))\frac{d}{dt}(1 - e^{-\eta t}) \\ &= \int_0^\infty dt \, (e^{-\eta t} - 1)(F_r(t) - F_p(t)),\end{aligned} \tag{23}$$

where $F_i(t) = h_i(\vec{q}(t))$ $(i = r \text{ or } p)$.

For the exchange reaction, the probability is given by $e^{-\eta\tau_p}$, where τ_p is the time the trajectory exists through the surface s_p. The probability is eventually obtained as[13]

$$\mathscr{P}_{exc} = \int_0^\infty dt \, (1 - h_p(\vec{q}(t))\frac{d}{dt}e^{-\eta t} = \int_0^\infty dt \, e^{-\eta t}F_p(t). \tag{24}$$

Inserting those probability functions into Eq. 5, the rate constants for the recombination and exchange reactions are given by

$$Q_r k_{cl}^{rec}(T,P) = \int_0^\infty dt \, e^{-\eta t}(C_{rr}^{cl}(t) - C_{rp}^{cl}(t)), \tag{25}$$

$$Q_r k_{cl}^{exc}(T,P) = \int_0^\infty dt \, e^{-\eta t}C_{rp}^{cl}(t), \tag{26}$$

where

$$C_{rr}^{cl}(t) = (2\pi)^{-f}\int d\vec{p}_1 \int d\vec{q}_1 \, e^{-\beta H(\vec{p}_1,\vec{q}_1)}F_r(\vec{p}_1,\vec{q}_1)F_r(\vec{p}(t),\vec{q}(t)), \tag{27}$$

$$C_{rp}^{cl}(t) = (2\pi)^{-f}\int d\vec{p}_1 \int d\vec{q}_1\, e^{-\beta H(\vec{p}_1,\vec{q}_1)} F_r(\vec{p}_1,\vec{q}_1) F_p(\vec{p}(t),\vec{q}(t)). \quad (28)$$

Here the relation

$$\int_0^\infty dt\, C_{rr}^{cl}(t) = \int_0^\infty dt\, C_{rp}^{cl}(t) \quad (29)$$

holds because in the limit $\eta \to 0$ the recombination rate should vanish.

The transcription of the rate constants to quantum mechanics simply involves replacing the classical correlation functions by their quantum mechanical counterparts. As in the classical case, the rate constants for recombination and exchange processes in quantum mechanics are thus given by

$$Q_r k_{rec}^{Y,M}(T,P) = \int_0^\infty dt\, e^{-\eta t}(C_{rr}^{Y,M}(t) - C_{rp}^{Y,M}(t)), \quad (30)$$

$$Q_r k_{exc}^{Y,M}(T,P) = \int_0^\infty dt\, e^{-\eta t} C_{rp}^{Y,M}(t). \quad (31)$$

Then, the flux–flux autocorrelation functions are given by

$$C_{rr}^{Y}(T) = \frac{1}{i\beta}\mathrm{tr}(e^{-\beta H}[h(s_r), F_r(t)]), \quad (32)$$

$$C_{rp}^{Y}(T) = \frac{1}{i\beta}\mathrm{tr}(e^{-\beta H}[h(s_r), F_p(t)]), \quad (33)$$

in Yamamoto's approach, while

$$C_{rr}^{M}(T) = \mathrm{tr}(F_r(0) e^{it_c{}^* H} F_r(0) e^{-it_c H}), \quad (34)$$

$$C_{rp}^{M}(T) = \mathrm{tr}(F_r(0) e^{it_c{}^* H} F_p(0) e^{-it_c H}), \quad (35)$$

in Miller's approach. Note that $F_i(0)$ ($i = r$ or p) is the quantum mechanical flux, which is again given by Eq. 11 with $\delta(s_i)$ and $h(s_i)$, instead of $\delta(s)$ and $h(s)$.

Because the rate constant is calculated by the Laplace transform of the flux–flux autocorrelation function, it is clear that the two approaches give different results. It is expected that they will coincide with each other in the classical limit, but the difference becomes large in the region where the λ integration in Eq. 18 cannot be ignored.

3 Numerical Calculations

In this section we calculate the (canonical) rate constants for recombination and exchange reactions using the Feynman path integral technique.[16] A huge calculation is usually required to obtain the exact matrix elements of propagators for a realistic system. Furthermore, it is necessary to consider some approximations and numerical techniques like Monte Carlo samplings[17] to perform it. Because the aim of this paper is to show how the rate constant in the Miller approach is different from that in the Yamamoto case, it would be more intuitive and useful to consider a simple system rather than a complicated case. We here study two analytically solvable cases: i.e., the free particle and the parabolic potential models in one-dimension, and leave more elaborate calculations for nontrivial cases for a forthcoming paper.

3.1 Free Particle Case. We first study the free particle case (see Fig. 3). The propagator for the free particle in a coordinate representation can be easily calculated by the path integral.[16] The matrix element of the flux operator F_i ($i = r$ or p) in coordinate space is also found easily for the free particle system. For details, see Appendix A.

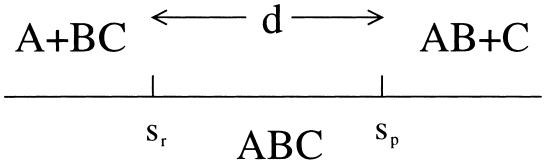

Fig. 3. Same as Fig. 2 but for the free particle case.

The flux–flux autocorrelation function in the Miller approach is eventually given by

$$C_{rp}^{M}(t) = \frac{1}{4\pi(t^2 + \beta^2/4)^{3/2}}\left[\frac{\beta}{2} + \frac{2mt^2d^2}{t^2 + \beta^2/4}\right] \times \exp\left[-\frac{m\beta d^2}{2(t^2 + \beta^2/4)}\right], \quad (36)$$

with d the distance between s_r and s_p (see Fig. 3). Note that the correlation depends on *only* the distance d and is independent of positions s_r and s_p, as it should be. From this expression the correlation function $C_{rr}^{M}(t)$ is easily obtained as

$$C_{rr}^{M}(t) = \frac{\beta}{8\pi(t^2 + \beta^2/4)^{3/2}}. \quad (37)$$

Those correlation functions are illustrated by the dotted curves in Figs. 4 and 5, in which we define $C_1 = md^2/2\beta$ and take $C_1 = 1.0$ to illustrate the correlation functions clearly. The rate constant for the reaction without recombination (i.e., in the limit $\eta \to 0$) can be obtained by the integral of Eq. 37 with respect to time (see Eq. 17):

$$Q_r k(T) = \int_0^\infty dt\, C_{rr}^{M}(t) = \frac{1}{2\pi\beta}. \quad (38)$$

By contrast, in the Yamamoto approach the flux–flux autocorrelation function is given by (see Appendix A)

$$C_{rp}^{Y}(t) = \frac{1}{2\pi\beta^2\sqrt{2t(t^2 + \beta^2)}}\exp\left[-\frac{m\beta d^2}{2(t^2 + \beta^2)}\right] \times \left[(\sqrt{t^2 + \beta^2} + t)^{3/2}\sin X + (\sqrt{t^2 + \beta^2} - t)^{3/2}\cos X\right], \quad (39)$$

where $X = m\beta^2d^2/2t(t^2 + \beta^2)$. This is not identical to Eq. 36. In particular, at short time it is divergent like $\sim 1/\sqrt{t}$ although it is integrable. Note that it again depends on only the distance d. If we set $s_r = s_p$ (or $d = 0$), we obtain[10]

$$C_{rr}^{Y}(t) = \frac{(\sqrt{t^2 + \beta^2} - t)^{3/2}}{2\sqrt{2t}\pi\beta^2(t^2 + \beta^2)^{1/2}}, \quad (40)$$

and, as expected, we can find that for the usual rate constant the Yamamoto correlation function gives $Q_r k(T) = 1/2\pi\beta$, which is the same as that in the Miller approach (see Eq. 38).

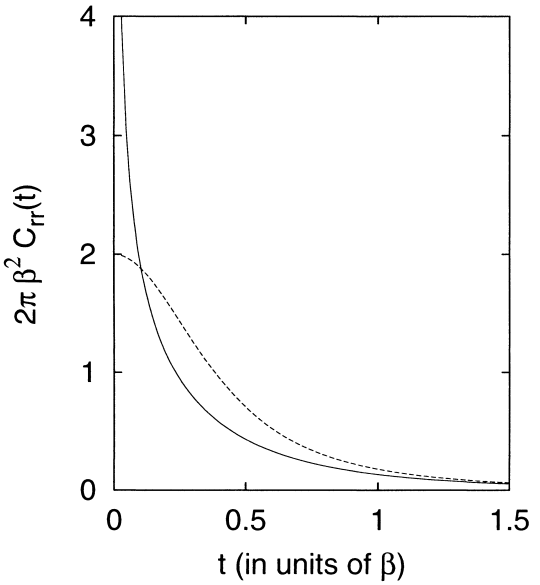

Fig. 4. Correlation function $C_{rr}(t)$ for the free particle. The dotted curve is for $C_{rr}^{M}(t)$, while the solid curve is for $C_{rr}^{Y}(t)$. We take $C_1 = md^2/2\beta = 1.0$.

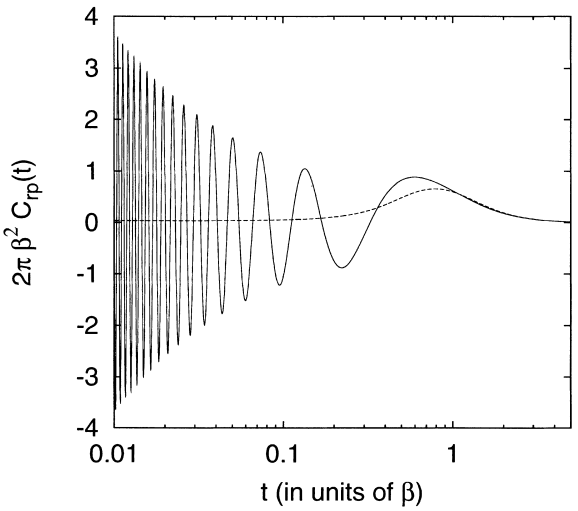

Fig. 5. Correlation function $C_{rp}(t)$ for the free particle. The dotted curve is for $C_{rp}^{M}(t)$, while the solid curve is for $C_{rp}^{Y}(t)$. We take $C_1 = md^2/2\beta = 1.0$.

Those correlation functions are shown by the solid curves in Figs. 4 and 5.

It can be seen from Figs. 4 and 5 that the interference effect in the correlation is taken into account correctly in the Yamamoto approach (although the vibrating behavior is inconvenient for numerical calculations). Contrastingly, in the Miller correlation function the interference is averaged and the shape is quite smooth. Thus, it is very convenient for actual computation. For the usual rate constant, the two approaches certainly give the same result, as we have seen above.

Next, we calculate the rate constants for recombination and exchange reactions. The rate constants are given by Eqs. 30 and 31. If we define the (*rr*)- and (*rp*)-rate constants by

$$Q_r k_{rr}^{Y,M} = \int_0^\infty \mathrm{d}t\, e^{-\eta t} C_{rr}^{Y,M}(t), \tag{41}$$

$$Q_r k_{rp}^{Y,M} = \int_0^\infty \mathrm{d}t\, e^{-\eta t} C_{rp}^{Y,M}(t), \tag{42}$$

the rate constants are given as $k_{rec}^{Y,M} = k_{rr}^{Y,M} - k_{rp}^{Y,M}$ and $k_{exc}^{Y,M} = k_{rp}^{Y,M}$.

Then, the Miller approach gives

$$Q_r k_{rr}^{M} = \frac{1}{8\pi\beta}\int_0^\infty \mathrm{d}x\, \frac{e^{-\alpha x}}{(x^2 + 1/4)^{3/2}}, \tag{43}$$

$$Q_r k_{rp}^{M} = \frac{1}{8\pi\beta}\int_0^\infty \mathrm{d}x\, e^{-\alpha x}\left[\frac{1}{(x^2 + 1/4)^{3/2}} + \frac{8C_1 x^2}{(x^2 + 1/4)^{5/2}}\right] \times \exp\left(-\frac{C_1}{x^2 + 1/4}\right), \tag{44}$$

where $x\ (= t/\beta)$ is a dimensionless variable and $\alpha = \beta\eta$, while in the Yamamoto approach we find

$$Q_r k_{rr}^{Y} = \frac{1}{2\sqrt{2}\pi\beta}\int_0^\infty \mathrm{d}x\, e^{-\alpha x}\, \frac{(\sqrt{x^2 + 1} - x)^{3/2}}{\sqrt{x(x^2 + 1)}}, \tag{45}$$

$$Q_r k_{rp}^{Y} = \frac{1}{2\sqrt{2}\pi\beta}\int_0^\infty \mathrm{d}x\, \frac{e^{-\alpha x}}{\sqrt{x(x^2 + 1)}} \exp\left[-\frac{C_1}{x^2 + 1}\right] \times \left[(\sqrt{x^2 + 1} + x)^{3/2}\sin X' + (\sqrt{x^2 + 1} - x)^{3/2}\cos X'\right], \tag{46}$$

with $X' = C_1/x(x^2 + 1)$.

In order to convert the collision frequency η to more familiar variables, we approximate the collisional deactivation rate constant by an expression given by the hard sphere collision theory. Furthermore, if one uses the ideal gas expansion, the frequency can be expressed by[13]

$$\eta = k_{deact}[M] = P\sqrt{\frac{2000}{T}} \times 10^{-11}, \tag{47}$$

with η in fs^{-1}, P in Pa and T in K. Then, we find

$$\alpha = \beta\eta \simeq 3.24 \times \frac{P}{T^{3/2}} \times 10^{-6}. \tag{48}$$

The factor C_1 is also converted as

$$C_1 = \frac{md^2}{2\beta} = 0.0103 \times ATd^2, \tag{49}$$

with A the reduced mass of the system in atomic mass units and d in Å. In this paper we consider a system which has a small reduced mass (like H + CO → HCO or H + O_2 → HO_2) to illustrate the difference between the two approaches clearly. In the following calculations, we thus take $A = 2$ and $d = 2$ Å and vary T and P.

Now we are in a position to show our results for the free particle case. First we define ratios

$$R_{rr}(T,P) = k_{rr}{}^{Y}/k_{rr}{}^{M}, \tag{50}$$

$$R_{rp}(T,P) = k_{rp}{}^{Y}/k_{rp}{}^{M}. \tag{51}$$

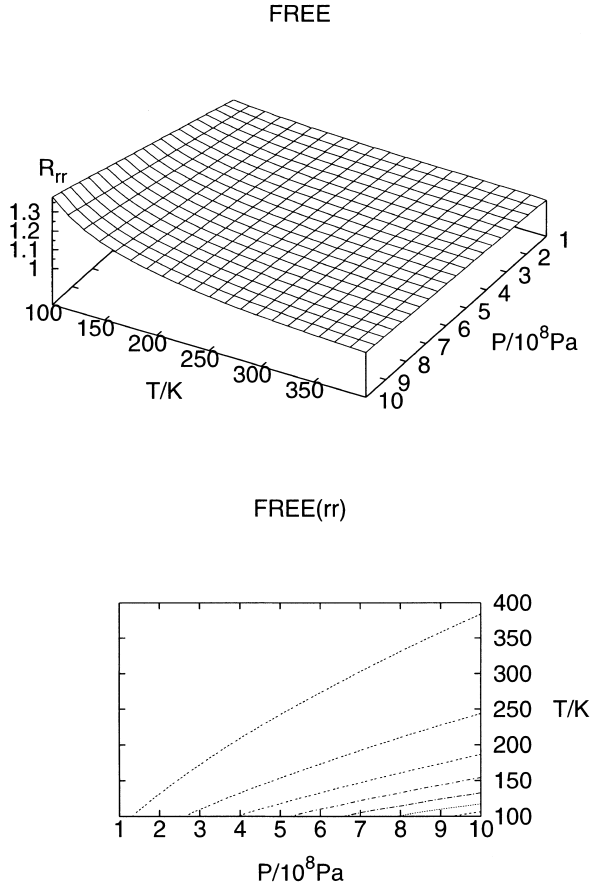

Fig. 6. Ratio of the (*rr*)-rate constants in the free particle case (top) and the contour plot (bottom). In the contour plot, the top dotted curve corresponds to $R_{rr} = 1.05$ and the other curves are plotted at intervals of 0.05. The bottom and right dotted curve is thus for $R_{rr} = 1.35$.

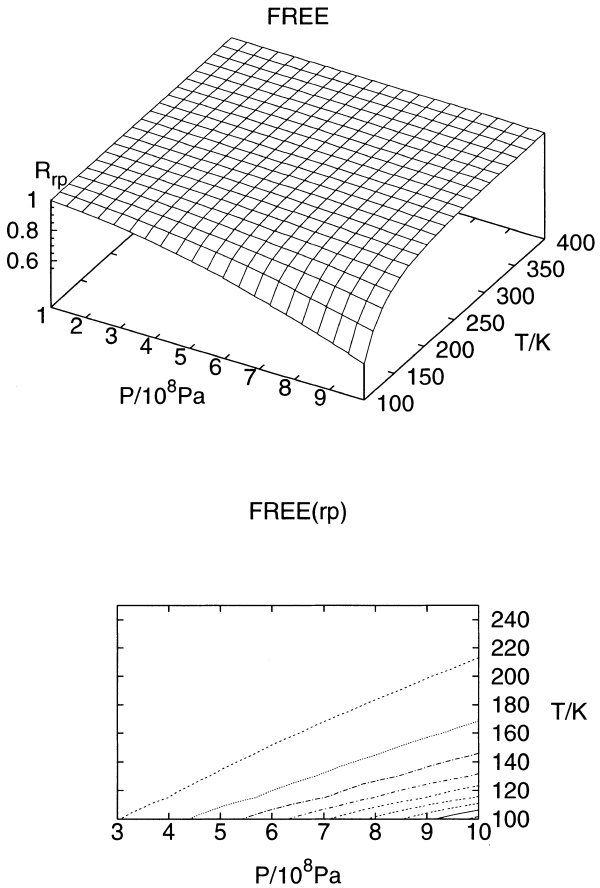

Fig. 7. Same as Fig. 6 but for the (*rp*)-rate constant. In the contour plot, the top dotted curve corresponds to $R_{rp} = 0.95$ and the other curves are plotted at intervals of 0.05. The bottom and right curve is for $R_{rp} = 0.55$.

Figures 6 and 7 illustrate the two ratios for the free particle case. Here we choose $T = 100$–400 K and $P = 0.1$–1 GPa. (To check the accuracy of the present numerical calculation, we have also evaluated the rate constant for the free particle with $\eta = 0$ and compared the result with the exact value given by Eq. 38. It is confirmed that the numerical calculation is sufficiently accurate.) In $R_{\rm rr}$, the ratio is enhanced at low T and high P, where quantum effects dominate, as we first expected in section 2. The ratio reaches 1.38 at $T = 100$ K and $P = 1$ GPa. Hence, the difference between the Yamamoto and the Miller approaches becomes rather large in the region of low T and high P. This tendency can be seen clearly in the contour plot of R_{rr}. On the contrary, in R_{rp} the ratio is reduced in the region where the quantum effect is strong. It is about 0.53 at $T = 100$ K and $P = 1$ GPa. The contour plot shows the decreasing behavior of R_{rp} at low T and high P.

Combining the (*rr*)- and (*rp*)-rate constants, one can calculate the ratio of the recombination rate constants, $R_{rec} = k^Y_{rec}/k^M_{rec}$. The ratio is presented in Fig. 8. (Note that the ratio for the exchange process is given by $R_{exc} = k^Y_{exc}/k^M_{exc} = R_{rp}$.) The behavior of R_{rec} seems similar to R_{rr} and the ratio again reaches 1.38 at $T = 100$ K and $P = 1$ GPa. From the contour plot we can see that there is a small difference between R_{rec} and R_{rr}.

3.2 Parabolic Potential Case. The second example is a reaction which occurs under a harmonic oscillator potential. We suppose that the potential has a frequency ω, the minimum point at x_0 with its value V_0, and s_r and s_p are located symmetrically with respect to the minimum point (see Fig. 9). The propagator for a particle moving under the potential can be found by the path integral.[16] The flux–flux autocorrelation function in the Miller approach is then calculated by (for details, see Appendix B)

$$C^M_{rp}(t) = \frac{\kappa^2 e^{-\beta V_0}}{4\pi\beta^2}\left[\frac{\sinh(\kappa/2)\cos u}{(\sinh^2(\kappa/2) + \sin^2 u)^{3/2}} + \kappa C_1 \frac{(\cosh(\kappa/2) + \cos u)^2 \sin^2 u}{(\sinh^2(\kappa/2) + \sin^2 u)^{5/2}}\right] \times \exp\left[-\kappa C_1 \frac{\sinh(\kappa/2)\,(\cosh(\kappa/2) + \cos u)}{\sinh^2(\kappa/2) + \sin^2 u}\right], \quad (52)$$

where $\kappa = \omega\beta$ and $u = \omega t$. Note that the correlation does not depend on the position of the minimum point explicitly. Similarly the correlation $C_{rr}{}^M$ is obtained as

$$C^M_{rr}(t) = \frac{\kappa^2 e^{-\beta V_0}}{4\pi\beta^2}\left[\frac{\sinh(\kappa/2)\cos u}{(\sinh^2(\kappa/2) + \sin^2 u)^{3/2}} - \kappa C_1 \frac{(\cosh(\kappa/2) - \cos u)^2 \sin^2 u}{(\sinh^2(\kappa/2) + \sin^2 u)^{5/2}}\right] \times \exp\left[-\frac{\kappa C_1 \sinh(\kappa/2)\,(\cosh(\kappa/2) - \cos u)}{\sinh^2(\kappa/2) + \sin^2 u}\right]. \quad (53)$$

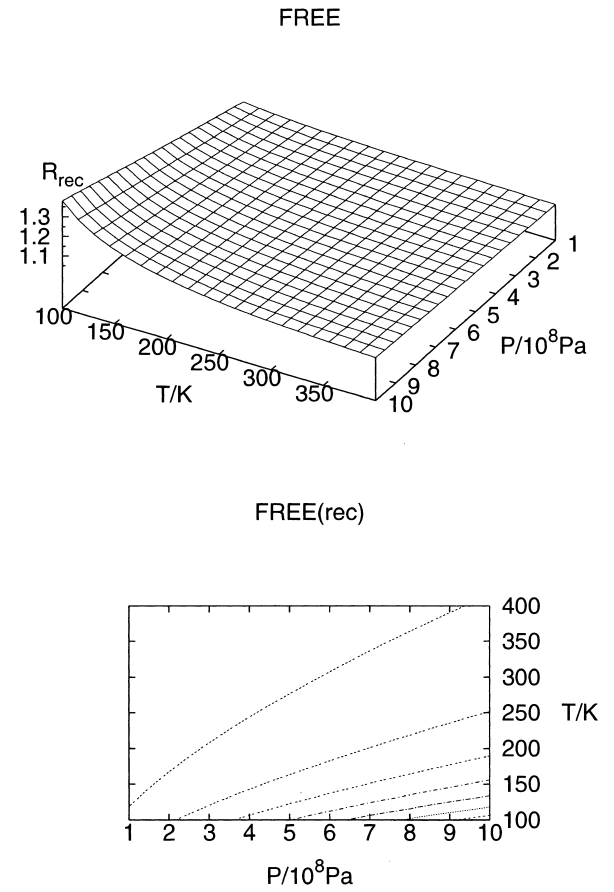

Fig. 8. Same as Fig. 6 but for the rate constant for the recombination reaction. In the contour plot, the top dotted curve corresponds to $R_{rec} = 1.05$ and the other curves are plotted at intervals of 0.05. The bottom and right curve is for $R_{rec} = 1.35$.

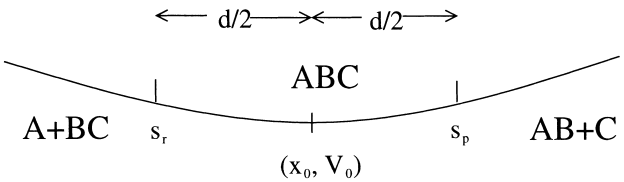

Fig. 9. Same as Fig. 2 but for the parabolic potential case. The minimum point is located at (x_0, V_0).

Those correlation functions are shown by the dotted curves in Figs. 10 and 11 (we take $C_1 = 1.5$ and $\kappa = 1.0$ to illustrate the correlation functions clearly). In the limit $\omega, V_0 \to 0$ Eqs. 52 and 53 are, of course, identical to Eqs. 36 and 37, respectively.

After lengthy algebra, we can find the correlation functions in the Yamamoto approach (for details, see Appendix B). For example, for $0 \leq u \leq \pi$, the correlations are expressed by

$$C_{rp}^{Y}(t) = \frac{\kappa e^{-\beta V_0}}{2\sqrt{2}\pi\beta^2 \sinh\kappa \sqrt{\sin u(\sinh^2\kappa + \sin^2 u)}} \times \exp\left[-\frac{\kappa C_1 \sinh\kappa(\cosh\kappa + \cos u)}{2(\sinh^2\kappa + \sin^2 u)}\right] \times \left[Z_{-}\cos\left(\frac{\kappa C_1}{2} Y_{+}\right) + Z_{+}\sin\left(\frac{\kappa C_1}{2} Y_{+}\right)\right], \quad (54)$$

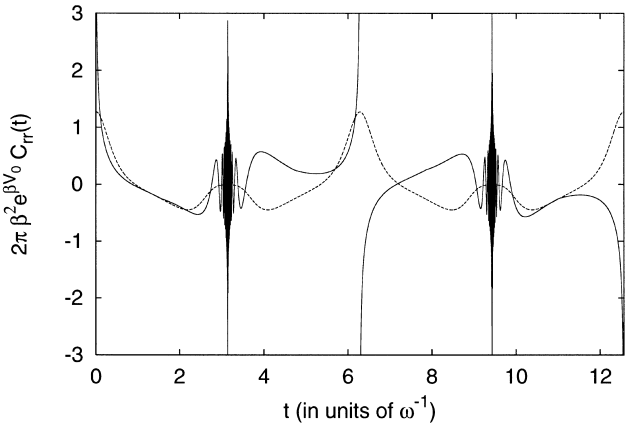

Fig. 10. Correlation function $C_{rr}(t)$ for the harmonic oscillator case. The dotted curve is for $C_{rr}^{M}(t)$, while the solid curve is for $C_{rr}^{Y}(t)$. We take $C_1 = 1.5$ and $\kappa = 1.0$.

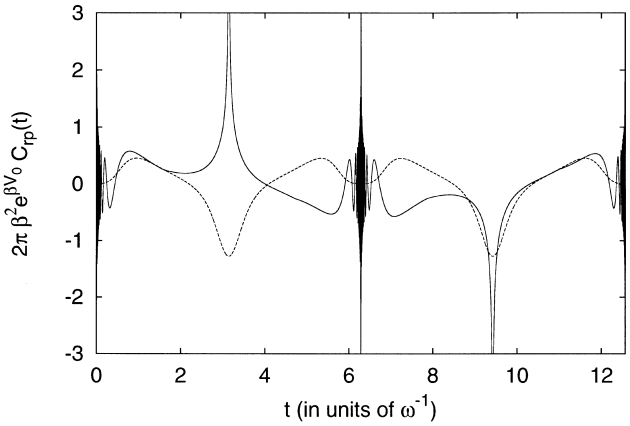

Fig. 11. Correlation function $C_{rp}(t)$ for the harmonic oscillator case. The dotted curve is for $C_{rp}^{M}(t)$, while the solid curve is for $C_{rp}^{Y}(t)$. We take $C_1 = 1.5$ and $\kappa = 1.0$.

and

$$C_{rr}^{Y}(t) = \frac{\kappa e^{-\beta V_0}}{2\sqrt{2}\pi\beta^2 \sinh\kappa \sqrt{\sin u(\sinh^2\kappa + \sin^2 u)}} \times \exp\left[-\frac{\kappa C_1 \sinh\kappa(\cosh\kappa - \cos u)}{2(\sinh^2\kappa + \sin^2 u)}\right] \times \left[Z_{-}\cos\left(\frac{\kappa C_1}{2} Y_{-}\right) - Z_{+}\sin\left(\frac{\kappa C_1}{2} Y_{-}\right)\right], \quad (55)$$

where

$$Z_{\pm} = (\sqrt{\sinh^2\kappa + \sin^2 u} \pm \sin u) \times (\sqrt{\sinh^2\kappa + \sin^2 u} \pm \cosh\kappa \sin u)^{1/2}, \quad (56)$$

$$Y_{\pm} = \frac{(1 \pm \cos u)\sinh^2\kappa - (\cosh\kappa - 1)\sin^2 u}{\sin u(\sinh^2\kappa + \sin^2 u)}. \quad (57)$$

Note that in the limit $\omega, V_0 \to 0$ the correlation functions approach those in the case of the free particle. Those correlation functions are also illustrated by the solid curves in Figs. 10

and 11.

One can see from the figures that the correct behavior of the correlation function is quite complicated and it is *divergent* (like $\sim 1/\sqrt{u}$) at $u = 0, \pi, 2\pi, \ldots$. However, the Miller correlation function is smooth *everywhere* and it *never* diverges. All those functions are periodical because of the harmonic oscillator potential and, as expected, the integral of the correlation function over one period vanishes.

The rate constants for recombination and exchange reactions are calculated by Laplace transforms of the correlation functions. In the Miller approach, the (*rr*)- and (*rp*)-rate constants are given by

$$Q_r k_{rr}^M = \frac{\kappa e^{-\beta V_0}}{4\pi\beta}\int_0^\infty du\left[\frac{\sinh(\kappa/2)\cos u}{(\sinh^2(\kappa/2)+\sin^2 u)^{3/2}} - \kappa C_1\frac{(\cosh(\kappa/2)-\cos u)^2\sin^2 u}{(\sinh^2(\kappa/2)+\sin^2 u)^{5/2}}\right] \times \exp\left[-\frac{\alpha}{\kappa}u - \frac{\kappa C_1\sinh(\kappa/2)(\cosh(\kappa/2)-\cos u)}{\sinh^2(\kappa/2)+\sin^2 u}\right]. \quad (58)$$

and

$$Q_r k_{rp}^M = \frac{\kappa e^{-\beta V_0}}{4\pi\beta}\int_0^\infty du\left[\frac{\sinh(\kappa/2)\cos u}{(\sinh^2(\kappa/2)+\sin^2 u)^{3/2}} + \kappa C_1\frac{(\cosh(\kappa/2)+\cos u)^2\sin^2 u}{(\sinh^2(\kappa/2)+\sin^2 u)^{5/2}}\right] \times \exp\left[-\frac{\alpha}{\kappa}u - \kappa C_1\frac{\sinh(\kappa/2)(\cosh(\kappa/2)+\cos u)}{\sinh^2(\kappa/2)+\sin^2 u}\right]. \quad (59)$$

Similarly, we can obtain the Yamamoto rate constants. Because the expression of the rate constant is, however, lengthy, we do not write it explicitly here (See Appendix B).

Now we show our results of the parabolic potential case. In Figs. 12 and 13, the ratios R_{rr} and R_{rp} are illustrated. In the present calculation, we fix κ to be 0.05, which means that the potential energy of the harmonic oscillator is much weaker (about 5%) than the typical thermal energy β^{-1}. We should note that the frequency ω is varied so as to keep $\kappa = 0.05$ at each T. If we set κ to be smaller than 0.05 (for example, $\kappa = 0.01$), the ratio, as it should, becomes close to that of the free particle case.

In Fig. 12, the ratio is again enhanced at low T and high P, which is similar to the result of the free particle case. The ratio at (T, P) = (100 K, 1 GPa) is about 1.38. One distinct feature in the parabolic case is an enhancement of the ratio in the region of high T and low P. This can also be seen in the contour plot. In such a region, the power α appearing in Laplace transform for the rate constant is small, and hence the rate constant at high T and low P is more influenced by the correlation function at large t than that at other T and P, that is, the rate constant is considerably affected by the (second) complicated structure around $u \simeq \pi$ in the correlation function (see Figs. 10 and 11). This is the reason why the enhancement at high T and low P appears in the ratio. The ratio at (T, P) = (400 K, 0.1 GPa) is about 1.11. In Fig. 13 a similar tendency can be seen: the ratio is reduced at low T and high P ($R_{rp} = 0.58$ at (T, P) = (100 K, 1 GPa)), which is similar to the free particle case, while it is enhanced at high T and low P ($R_{rp} = 1.43$ at (T, P) = (400 K, 0.1 GPa)).

Combining the (*rr*)- and (*rp*)-rate constants, we can calculate the rate constant for the recombination process; this is presented in Fig. 14. In R_{rec}, the ratio is enhanced at low T and high P ($R_{rec} = 1.38$ at (T, P) = (100 K, 1 GPa)), while it is reduced at high T and low P ($R_{rec} = 0.38$ at (T, P) = (400 K, 0.1 GPa)). This behavior is also seen in the contour plot.

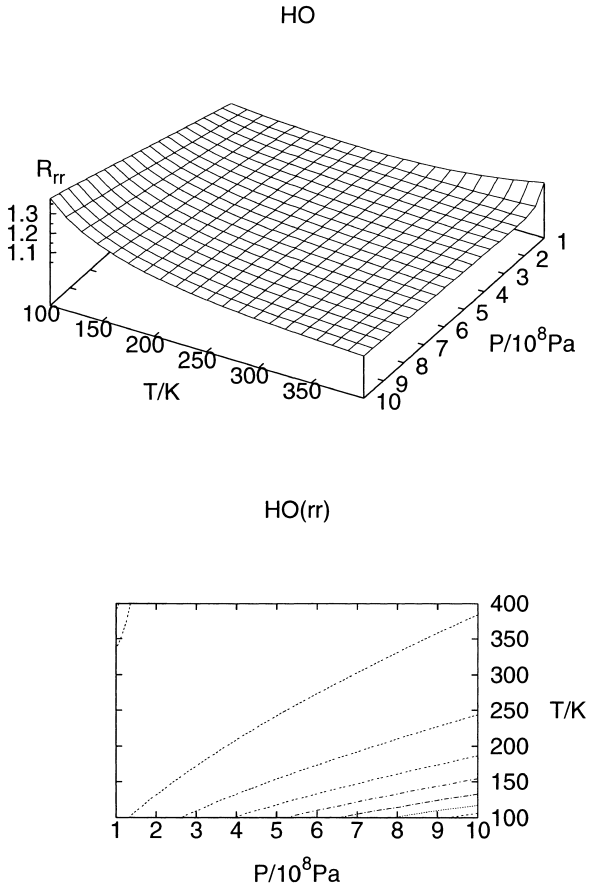

Fig. 12. Ratio of the (*rr*)-rate constants under the harmonic oscillator potential with $\kappa = 0.05$ (top) and the contour plot (bottom). In the contour plot, the dotted curve connecting (T, P) = (100 K, 0.14 GPa) and (380 K, 1 GPa) corresponds to $R_{rr} = 1.05$. The top, left dotted curve connecting (T, P) = (340 K, 0.1 GPa) and (400 K, 0.14 GPa) is also for $R_{rr} = 1.05$. The other curves are plotted at intervals of 0.05. The bottom and right dotted curve is thus for $R_{rr} = 1.35$.

4 Summary and Conclusion

The exact quantum mechanical expression for thermal reaction rates can be formulated by the linear response theory,[7,8] which Yamamoto first discussed in the early 60's.[6] Later, in the early 70's, Miller et al.[5,9] have independently proposed a more convenient way to perform numerical computation, which can provide the exact rate constant in the limit that the dynamics of the system is extended to $t \to \infty$.

We have studied the difference between the two approaches in thermal reactions which involve exchange and recombination processes. Because the rate constants in those reactions are calculated by Laplace transforms of the flux-flux autocorrelation functions, the results evaluated by the two approaches are different. In this paper, we have considered two solvable cases, i.e., the free particle and parabolic potential models, to demonstrate the difference intuitively. We have found that the shapes of the correlation functions are quite different in the two approaches and that the difference of the rate constants appears in the region where quantum effects dominate. In both

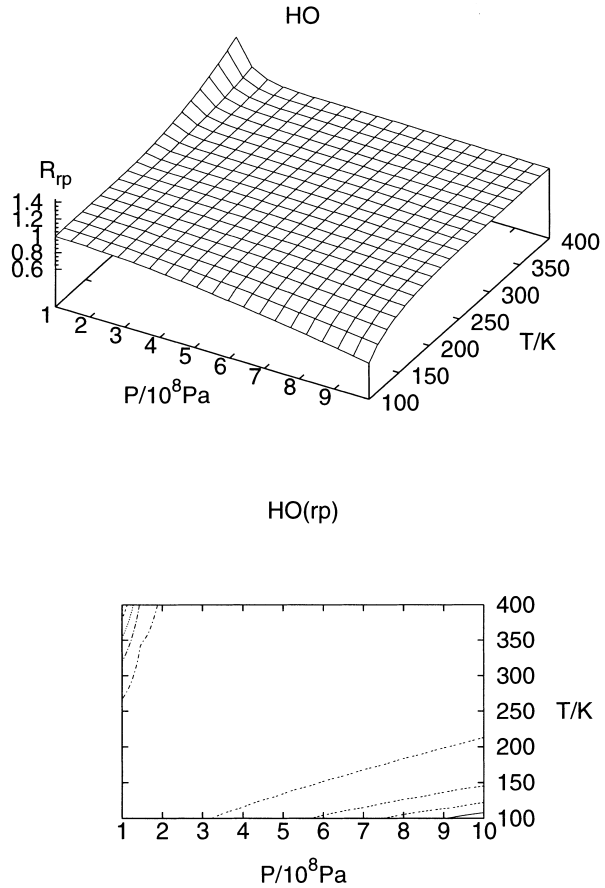

Fig. 13. Same as Fig. 12 but for the (*rp*)-rate constant. In the contour plot, the dotted curve connecting (T, P) = (100 K, 0.33 GPa) and (210 K, 1 GPa) corresponds to R_{rp} = 0.95, while the dot-dashed curve connecting (T, P) = (270 K, 0.1 GPa) and (400 K, 0.19 GPa) is for R_{rp} = 1.05. The other curves are plotted at intervals of 0.1. The bottom and right curve is for R_{rp} = 0.65.

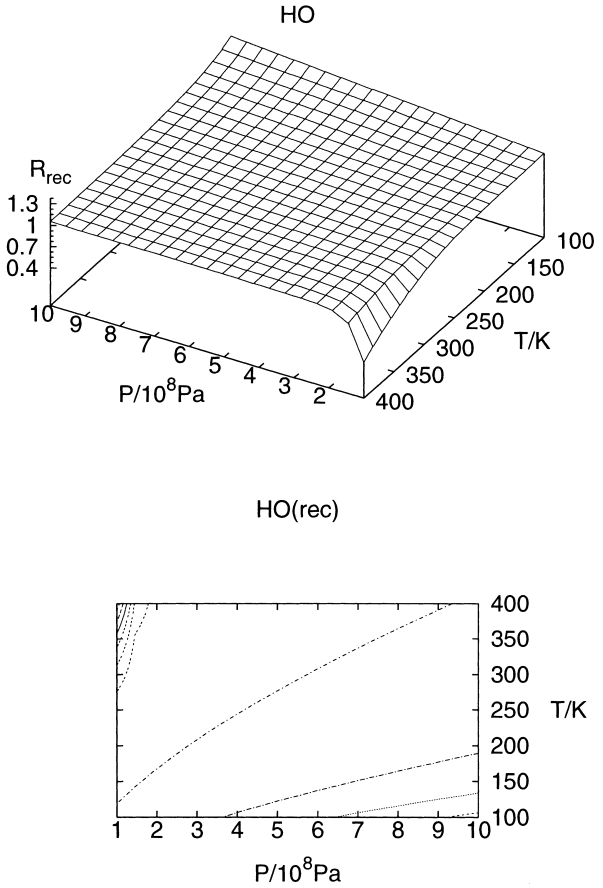

Fig. 14. Same as Fig. 12 but for the rate constant for the recombination reaction. In the contour plot, the dot-dashed curve connecting (T, P) = (120 K, 0.1 GPa) and (400 K, 0.93 GPa) corresponds to R_{rec} = 1.05, while the dotted curve connecting (T, P) = (275 K, 0.1 GPa) and (400 K, 0.18 GPa) is for R_{rec} = 0.95. The other curves are plotted at intervals of 0.1. The bottom and right curve is for R_{rec} = 1.35.

the free and parabolic cases, the rate constant for recombination in the Yamamoto approach is larger than that in the Miller approach; the enhancement becomes about 40% at low temperature and high pressure.

In conclusion, the Miller method is certainly an economical and powerful tool to perform numerical calculations for thermal rates of realistic reactions. However, it may underestimate the rate constants for recombination and exchange processes in the region where quantum effects dominate, because of neglecting the λ integral appearing in the Kubo identity.

Appendix

Appendix A—Free Particle Case. The matrix element of the flux operator F_i (i = r, or p) in the coordinate representation is given by[9]

$$\langle u|F_i|u'\rangle = \frac{1}{2im}[\delta'(u - s_i)\delta(u' - s_i) - \delta(u - s_i)\delta'(u' - s_i)]. \tag{60}$$

Using this expression, one can evaluate the flux–flux autocorrelation function in the Miller approach as

$$\begin{aligned} C_{rp}^{M}(T) &= \mathrm{tr}(F_r(0)e^{it_c^* H}F_p(0)e^{-it_c H}), \\ &= -\frac{1}{2m^2}\Re\left[\frac{\partial}{\partial u}\langle u|e^{-iHt_c}|u'\rangle^{\star}\frac{\partial}{\partial u'}\langle u|e^{-iHt_c}|u'\rangle\right. \\ &\quad \left. - \langle u|e^{-iHt_c}|u'\rangle^{\star}\frac{\partial^2}{\partial u\partial u'}\langle u|e^{-iHt_c}|u'\rangle\right]_{u\,=\,s_r,\,u'\,=\,s_p}, \end{aligned} \tag{61}$$

where $t_c = t - i\beta/2$ and $\Re$ stands for taking the real part. On the other hand, the Yamamoto correlation function is given by

$$\begin{aligned} C_{rp}^{Y}(T) &= \frac{1}{i\beta}\mathrm{tr}(e^{-\beta H}[h(s_r), F_p(t)]), \\ &= \frac{1}{m\beta}\Im\int_{s_r}^{\infty}du\left[i\langle u|e^{-iHt_\beta}|u'\rangle^{\star}\frac{\partial}{\partial u'}\langle u|e^{-iHt}|u'\rangle\right. \\ &\quad \left. - i\langle u|e^{-iHt}|u'\rangle\frac{\partial}{\partial u'}\langle u|e^{-iHt_\beta}|u'\rangle^{\star}\right]_{u'\,=\,s_p}, \end{aligned} \tag{62}$$

where $t_\beta = t - i\beta$ and $\Im$ stands for the imaginary part.

With use of the path integral technique,[16] the propagator for

the free particle at finite β is calculated by

$$\left\langle u\middle|e^{-iHt_\beta}\middle|u'\right\rangle = \sqrt{\frac{m}{2\pi i}}\frac{e^{i\theta/2}}{(t^2+\beta^2)^{1/4}} \times \exp\left[\frac{m(it-\beta)}{2(t^2+\beta^2)}(u-u')^2\right], \tag{63}$$

where

$$\cos\theta = \frac{t}{\sqrt{t^2+\beta^2}} \text{ and } \sin\theta = \frac{\beta}{\sqrt{t^2+\beta^2}}. \tag{64}$$

We can easily calculate the correlation functions using those expressions. The final results are explicitly presented in Eqs. 36–40.

Appendix B—Parabolic Potential Case. The propagator for a particle moving under the harmonic oscillator potential (at finite β) which has the minimum point at (x_0, V_0) (see Fig. 9) is evaluated by[16]

$$\left\langle u\middle|e^{-iHt_\beta}\middle|u'\right\rangle = \sqrt{\left(\frac{m\omega}{2\pi i}\right)\frac{\cosh\kappa\sin u + i\sinh\kappa\cos u}{\sinh^2\kappa+\sin^2 u}}e^{-\beta V_0} \times \exp\left[im\omega\left(\frac{\sin u\cos u + i\sinh\kappa\cosh\kappa}{2(\sinh^2\kappa+\sin^2 u)}\right)(u^2+u'^2) - im\omega\left(\frac{\cosh\kappa\sin u + i\sinh\kappa\cos u}{\sinh^2\kappa+\sin^2 u}\right)uu' - iV_0t\right], \tag{65}$$

where $\kappa = \omega\beta$, $u = \omega t$ and $t_\beta = t - i\beta$.

Because it is easy to calculate the Miller correlation function using Eqs. 61 and 65, we do not show its derivation here. The final result is given in Eqs. 52 and 53. Instead, we explicitly present the Yamamoto correlation function. It is a periodical function and the period is 4π (see Figs. 10 and 11). Then, we divide it into 4 parts. Using Eqs. 62 and 65, we find:
(1) for $0 \le u \le \pi$, the results are given by Eqs. 54 and 55.
(2) for $\pi < u \le 2\pi$,

$$C_{rr}^Y(t) = \frac{\kappa e^{-\beta V_0}}{2\sqrt{2}\pi\beta^2\sinh\kappa\sqrt{|\sin u|(\sinh^2\kappa+\sin^2 u)}} \times \exp\left[-\frac{\kappa C_1\sinh\kappa(\cosh\kappa-\cos u)}{2(\sinh^2\kappa+\sin^2 u)}\right] \times \left[Z_+\cos\left(\frac{\kappa C_1}{2}Y_-\right) - Z_-\sin\left(\frac{\kappa C_1}{2}Y_-\right)\right], \tag{66}$$

and

$$C_{rp}^Y(t) = \frac{\kappa e^{-\beta V_0}}{2\sqrt{2}\pi\beta^2\sinh\kappa\sqrt{|\sin u|(\sinh^2\kappa+\sin^2 u)}} \times \exp\left[-\frac{\kappa C_1\sinh\kappa(\cosh\kappa+\cos u)}{2(\sinh^2\kappa+\sin^2 u)}\right] \times \left[Z_+\cos\left(\frac{\kappa C_1}{2}Y_+\right) + Z_-\sin\left(\frac{\kappa C_1}{2}Y_+\right)\right], \tag{67}$$

where $Z_\pm$ and $Y_\pm$ are defined by Eqs. 56 and 57.
(3) for $2\pi < u \le 3\pi$,

$$C_{rr}^Y(t) = \frac{\kappa e^{-\beta V_0}}{2\sqrt{2}\pi\beta^2\sinh\kappa\sqrt{\sin u(\sinh^2\kappa+\sin^2 u)}} \times \exp\left[-\frac{\kappa C_1\sinh\kappa(\cosh\kappa-\cos u)}{2(\sinh^2\kappa+\sin^2 u)}\right] \times \left[-Z_-\cos\left(\frac{\kappa C_1}{2}Y_-\right) + Z_+\sin\left(\frac{\kappa C_1}{2}Y_-\right)\right], \tag{68}$$

and

$$C_{rp}^Y(t) = \frac{\kappa e^{-\beta V_0}}{2\sqrt{2}\pi\beta^2\sinh\kappa\sqrt{\sin u(\sinh^2\kappa+\sin^2 u)}} \times \exp\left[-\frac{\kappa C_1\sinh\kappa(\cosh\kappa+\cos u)}{2(\sinh^2\kappa+\sin^2 u)}\right] \times \left[-Z_-\cos\left(\frac{\kappa C_1}{2}Y_+\right) - Z_+\sin\left(\frac{\kappa C_1}{2}Y_+\right)\right]. \tag{69}$$

(4) for $3\pi < u \le 4\pi$,

$$C_{rr}^Y(t) = \frac{\kappa e^{-\beta V_0}}{2\sqrt{2}\pi\beta^2\sinh\kappa\sqrt{|\sin u|(\sinh^2\kappa+\sin^2 u)}} \times \exp\left[-\frac{\kappa C_1\sinh\kappa(\cosh\kappa-\cos u)}{2(\sinh^2\kappa+\sin^2 u)}\right] \times \left[-Z_+\cos\left(\frac{\kappa C_1}{2}Y_-\right) + Z_-\sin\left(\frac{\kappa C_1}{2}Y_-\right)\right], \tag{70}$$

and

$$C_{rp}^Y(t) = \frac{\kappa e^{-\beta V_0}}{2\sqrt{2}\pi\beta^2\sinh\kappa\sqrt{|\sin u|(\sinh^2\kappa+\sin^2 u)}} \times \exp\left[-\frac{\kappa C_1\sinh\kappa(\cosh\kappa+\cos u)}{2(\sinh^2\kappa+\sin^2 u)}\right] \times \left[-Z_+\cos\left(\frac{\kappa C_1}{2}Y_+\right) - Z_-\sin\left(\frac{\kappa C_1}{2}Y_+\right)\right]. \tag{71}$$

As shown in Figs. 10 and 11, there is a symmetry property: $C_{ri}^Y(0 \le u \le \pi) = -C_{ri}^Y(2\pi < u \le 3\pi)$ and $C_{ri}^Y(\pi \le u \le 2\pi) = -C_{ri}^Y(3\pi < u \le 4\pi)$ ($i = r$ or p). Thus, it is enough to calculate the correlation function in the region of $0 \le u \le 2\pi$. The rate constants are calculated by Laplace transforms of those periodical correlation functions.

References

1 See, for example: S. L. Mielke, D. G. Truhlar, and D. W. Schwenke, *J. Phys. Chem.*, **98**, 1053 (1994).

2 See, for example: A. Kuppermann, *J. Phys. Chem.*, **100**, 2621 (1996).

3 See, for example: D. G. Truhlar, W. L. Hase, and J. T. Hynes, *J. Phys. Chem.*, **87**, 2664 (1983).

4 P. Pechukas and F. McLafferty, *J. Chem. Phys.*, **58**, 1622 (1973); *J. Chem. Phys. Lett.*, **27**, 511 (1974); D. G. Truhlar and A. Kuppermann, *J. Chem. Phys.*, **56**, 2232 (1972); D. G. Truhlar, A. Kuppermann, and J. T. Adams, *J. Chem. Phys.*, **59**, 395 (1973).

5 W. H. Miller, *J. Chem. Phys.*, **61**, 1823 (1974); *J. Chem. Phys.*, **62**, 1899 (1975).

6 T. Yamamoto, *J. Chem. Phys.*, **33**, 281 (1960). See also, P. G. Wolynes, *Phys. Rev. Lett.*, **47**, 968 (1981).

7 R. Kubo, *J. Phys. Soc. Japan*, **12**, 570 (1957); R. Kubo, M. Yokota, and S. Nakajima, *J. Phys. Soc. Japan*, **12**, 1203 (1957).

8 H. Mori, *J. Phys. Soc. Japan*, **11**, 1029 (1956).

9 W. H. Miller, S. D. Schwartz, and J. W. Tromp, *J. Chem. Phys.*, **79**, 4889 (1983).

10 See, for example: W. H. Miller, *J. Phys. Chem.*, **102**, 793 (1998).

11 K. Yamashita and W. H. Miller, *J. Chem. Phys.*, **82**, 5475 (1985). T. J. Park and J. C. Light, *J. Chem. Phys.*, **91**, 974 (1989).

12 See, for example: W. H. Miller, *J. Phys. Chem.*, **99**, 12387 (1995).

13 T. C. Germann and W. H. Miller, *J. Phys. Chem.*, **101**, 6358 (1997).

14 J. Qi and J. M. Bowman, *J. Phys. Chem.*, **100**, 15165 (1996); V. A. Mandelshtam, H. S. Taylor, and W. H. Miller, *J. Chem. Phys.*, **105**, 496 (1996).

15 J. A. Miller, R. J. Kee, and C. K. Westbrook, *Annu. Rev. Phys. Chem.*, **41**, 345 (1990); P. O. Wennberg, R. C. Cohen, R. M. Stimpfle, J. P. Koplow, J. G. Anderson, R. J. Salawitch, D. W. Fahey, E. L. Woodbridge, E. R. Keim, R. S. Gao, C. R. Webster, R. D. May, D. W. Toohey, L. M. Avallone, M. H. Proffitt, M. Loewenstein, J. R. Podolske, K. R. Chan, S. C. Wofsy, *Science*, **266**, 398 (1994).

16 R. P. Feynman and A. R. Hibbs, "Quantum Mechanics and Path Integrals," McGraw-Hill, New York (1965).

17 C. Leforestier and W. H. Miller, *J. Chem. Phys.*, **100**, 733 (1994); W. H. Thompson and W. H. Miller, *J. Chem. Phys.*, **106**, 142 (1997).